HYDRODYNAMICS ANALYSIS OF MARINE AMPHIBIOUS AIRCRAFT L8 HULL BY FLUENT SOFTWARE

M, Safari[1] , M.R., Moghoomi[2]

[1] Department of Mechanical Engineering,
Arak University of Technology, Arak, Iran.

[2] Department of Mechanical Engineering,
Daneshpajoohan Higher Education Institute, Isfahan, Iran.

Email: [*1]m.safari@arakut.ac.ir; [2]moghoomi@yahoo.com

ABSTRACT: Nowadays, design and manufacturing of amphibious aircrafts known as a flying boat are embraced in the maritime transport industries, military usage and relay. Although such flying vessels have been arranged in the new technologies of marine industries but the researchers and designers are able to become the owners of design-engineering science of amphibious marine vessels in the shortest, possible time. In view of prevailing equations on computational fluids and hydrodynamic of air-sea amphibious aircraft movement, this paper analyzed a sample of these vessels species with 4°, 6°, 8° angles of attack of the underside of the aircraft airfoil and action of two types, laminar and turbulent Reynolds flow was taken. The results showed that the lift and drag coefficients in two laminar and turbulent conditions were proportional to the dynamic stability and consistent with experimental design and manufacturing and represented the stability of the flying vessel in two laminar and turbulent flow.

KEYWORDS: *Amphibious aircrafts, Drag coefficient, Angle of attack, Lift coefficient, Airfoil.*

1.0 INTRODUCTION

Flying boats or surface effect instruments are assumed a type of amphibious sea-air devices which use the surface effect phenomenon while having the ability to land on water and take off from the water surface in which they increase their operational capabilities. Due to the special design of these devices. it can be said that the flying boat is not an aircraft given the ability to sit on water but it is a boat which has been given the flying ability while using a simple physical phenomenon (in terms of operational expectations). It should be noted that some types of fast boats also benefit from such phenomenon. A surface effect vessel can be described as a marine vehicle which flies over water surface and with a small distance towards it and it can reach speeds over 60 Knote, about 100

kilometers per hour. So far, many researchers have investigated hydrodynamic stability and instability of airfoils and vesseling objects. A study [1] has addressed numerical analysis and simulation of one type of aircraft. The authors have analyzed barriers which caused vortex and spiral structures and cause disorder. Another study[2] investigates the created vortexes in wind tunnel at high, average and low flying speeds by experimenting a sample of flying boats. A study uses Saekeeper software to determine the added mass force of the ship and compare the value of this force for different shapes to analyze the body form of a sample vessel [3]. In another study[4], a proposal was suggested which suits for different types of vessels in order to optimize them. The effect of thrust angle on body-propeller-rudder reaction has been studied and the findings yield that changing of thrust angle and length change of the upstream body flow with high accuracy. Calculated results have been compared to the wind tunnel in which the propeller thrust, rotation and rudder forces have been investigated [5].

In another study, an interaction of hydrodynamic and hydro acoustic in the propeller and rudder of the vessels is analyzed and the authors conclude that if they extend this research, appropriate measures can be taken to practically separate hydrodynamic and acoustic surfaces of the pressure fluctuations and fluids dynamic variations [6]. In addition to the above studies, some papers have focused on the design of body of marine amphibious aircrafts[7,8] . The laser forming of a doubly curved saddle shape is analyzed experimentally and numerically [7]. The results yield that curvatures associated with obtained saddle shape created by spiral irradiating scheme are considerably large and a considerable and suitable symmetry was produced in the obtained saddle shape with spiral irradiating scheme. Another study investigates the laser forming of metallic dome-shaped parts using spiral and radial-circular scan paths[8]. The results show that the stress distribution is more uniform in laser forming with the use of spiral scanning path. In addition, the deformed parts with spiral scanning path are more uniform compared to other investigated scanning paths. Research methodology in this paper is the way that the prevailing equations on vessels engineering are firstly analyzed and then the Fluent software is used by simulating the airfoil sections in the vertical plane and then the same airfoil will be analyzed from the front view. A sample of an amphibious aircraft is illustrated in Figure 1.

Figure 1: A sample of a flying boat (amphibious aircraft)

2.0 ENGINEERING EQUATIONS

2.1 Mathematical equations and simulating analysis

Force lift 1 is presented by Equation1 as follows:

$$F_L = 1/2 C_L \rho U^2 A \quad (1)$$

In Equation 1, U is the vessel speed, ρ is the density, A is the airfoil area and C_L is the lift coefficient which its functionality with effecting factors on this coefficient is as Equation 2:

$$C_L = f(\rho, \mu, D, \alpha) \quad \text{OR} \; C_L = f(Re_d, \alpha) \quad (2)$$

$$C_L = f(\rho, \mu, D, \alpha)$$

It should be noted that the angle of attack (α) determines the condition of surface stands in front of the flow. The lift force 2 is a frictional force and is a combination of viscosity or tangent and pressure and it is calculated from Equation 3 as follows:

$$\vec{F}_{D\,tot} = \vec{F}_P + \vec{F}_\mu = \int_A -P dA + \int_A \tau_m dA \quad (3)$$

Therefore, in general the drag force can be calculated by Equation 4 as follows:

$$F_L = \frac{1}{2} C_{D\,tot} \rho U^2 A \quad (4)$$

In Equation 4, $C_{D\,tot}$ is called the total drag coefficient. Also, the effective lift coefficient in the fluid flow on the boat airfoil blade can be calculated from Equation 5 as follows:

$$C_l = \frac{L}{1/2\rho.A_r.U^2} \tag{5}$$

In Equation 5, C_l is the lift coefficient, ρ is the sea water density, A_r is the airfoil area and U is the vessel speed. In Figure 2 geometrical specifications of the lower airfoil of the flying boat is shown. It should be explained that the geometric information of this investigated airfoil geometry is obtained from Ref. [7].

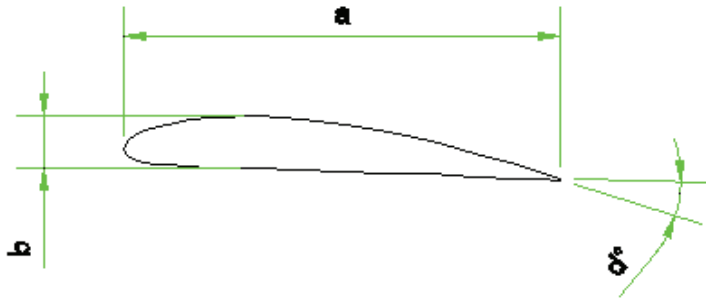

Figure 2: Geometrical parameters of the flying boat lower airfoil

In addition to lift coefficient, another parameter that is effective on airfoil design is the Drag coefficient that is calculated from equation 6 as follows:

$$C_d = \frac{D}{1/2\rho.\mathrm{A}_r.U^2} \tag{6}$$

In Equation 6, C_d is the Drag co-efficient. The rudder torque coefficient is achievable from equation 7 as follows:

$$C_Q = \frac{QR}{\frac{1}{2}\rho.\mathrm{V}^2.A_R.C_m} \tag{7}$$

In Equation 7, C_m is the momentum coefficient that is calculated from Equation 8 as follows:

$$C_m = \frac{A_R}{b} \tag{8}$$

In the above equations, ρ is the density, V is the rudder or vessel speed, A_r is the airfoil area, C_l is the lift coefficient, C_d is the Drag coefficient and C_Q is the torque coefficient [10].

Besides, in Equation 9 the airfoil vertical force coefficient is calculated as follows:

$$C_N = \frac{F}{1/2\rho.\,\mathrm{A}_r.U^2} = C_L cos\alpha + C_D sin\alpha \tag{9}$$

The airfoil area (A_r) is calculated in Equation10 as follows:

$$\mathrm{A}_r = \bar{b}.\bar{c} \tag{10}$$

In Equation 10, $\bar{b}$ and $\bar{c}$ are the airfoil blade average height and the chord length respectively. One of the other coefficients is the aspect ratio that is calculated from Equation 11.

$$A.R. = \frac{\bar{b}}{\bar{c}} \tag{11}$$

In Figures 3 and 4 the schematics of airfoil blade are shown.

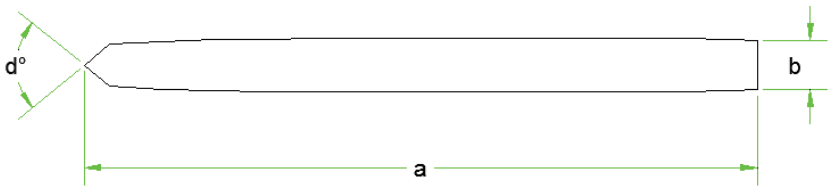

Figure 3: Vertical view of the airfoil

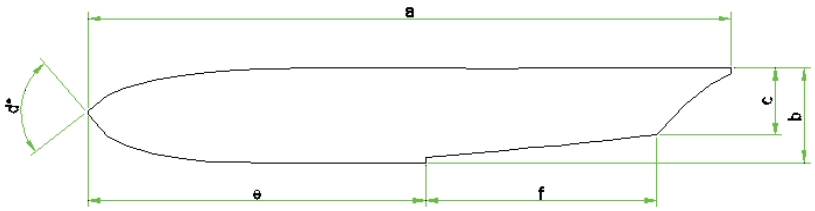

Figure 4: Front view of the flying boat airfoil section

2.2 Investigating the lift and drag coefficient with analytical method

C_L, C_D and C_{QN} could be considered as below by using experimental equations and calculations:

For the time when the angle of attack is less than stall angle we have:

$$C_L = C_{L1} + C_{L2} = 2\pi . \frac{AR.(AR+0.7)}{(AR+0.7)^2} .\text{Sin}\ \alpha + C_Q .\sin\alpha .\sin\alpha.\cos\alpha \quad (12)$$

$$C_D = C_{D1} + C_{D2} + C_{D0} = \frac{C_L^2}{\pi AR} + C_Q .(\cos\alpha)^3 + C_{D0} \quad (13)$$

$$C_{QN} = -(CL_{10}\ \cos\alpha + CD_{10}\sin\alpha).(0.47 - \frac{AR+2}{4(AR+1)}) - 0.75(CL_{10}\cos\alpha + CD_{10}\sin\alpha) \quad (14)$$

The first sentence in equation (12) is achieved from the thin foil potential theory which is accurate for zero or infinite aspect ratio and for other values the aspect ratio is approximate. The first term in equation 13 is related to induced drag achieved from the vortexes behind the rudder. The first term in equation 14 is also related to the condition when the fluid is ideal. The second term in equation 12 and 13 is related to extra resistance which has been considered as the fourth power of the speed. In case of rudders which have sharp edges, the Q_N value can be considered equivalent to number 1, otherwise this number will be larger than 1. The second term in equation 14 has been achieved from considering the force standing in distance of 0.75 * chord length from the attack edge. Besides, to calculate the friction coefficient we use equation 15:

$$C_{D0} = 2.5 \frac{0.75}{(\log R_n - 2)^2} \quad (15)$$

These equations are appropriate for the time when half of the airfoil area is soaked. For better understanding of the equations, it should be said that intended purpose has been the same three types of drags which have been added and the total drag force is the summation of 4 skin-friction drag 5 spray drag, 6 form drag and 7 induced drag. Based on this, the drag angle can be considered as equation 16:

$$C^*_D = C^*_{D0} + C^*_{Di} = \frac{D^*}{1/2\rho . A_r . U^2} \quad (16)$$

In this equation, C^*_D is the summation of skin-friction drag, spray and form drag coefficients and also C^*_{Di} is the induced drag coefficient. If the profile thickness is more, the maximum lift coefficient increases. From disadvantages of thickness rise, drag increase and also increase in cavitation likelihood could be pointed out. The conclusion is that mentioned equations are suitable for the angles less than stall angle, otherwise, the flow separation occurs and the mentioned equations will not be credible. In summary, the profile shape aspect ratio and the thickness of the Reynolds number of the surface roughness of the inlet fast distribution turbulence could be recognized as effective parameters on stall angle. In the presence of the mentioned four latest cases, the maximum lift coefficient in wind tunnel or the stretch pool cannot be achieved.

3.0 SOFTWARE ANALYSIS OF THE AIRFOIL

In this paper, hydrodynamic investigation of the L8Hull flying vessel with NACA4412 airfoil section and the chord length of 20 inches and the wing length of 83.826 were addressed. Water estuary of this vessel was considered 3 inches and during the checking of offset table related to the airfoil section of this vessel which is now in hands of the laboratory associated to NACA firm was simulated and analyzed in Fluent. It should be explained that this offset table and the conducted analysis are related to one laboratory model and unfortunately the information related to the manufactured model is not accessible and we only rely on the analysis of this laboratory model. The analysis was in two dimension scales and the curves under the vessel which had been accurately specified in offset table were not included.

Firstly, the aircraft airfoil and then its body were addressed. This study was conducted for two laminar and turbulent flow types.

1. For the laminar flow condition: where the air speed was 8.34 m/s and the water speed was 5 m/s. This simulation was also conducted for three types of airfoil angle of attack 4°, 6° and 8°(the lower part and in contact with flying boat).

a) For angle of attack of α=4°, the achieved coefficients are C_d=1.314*1000 (drag coefficient) and C_l=1.314*1000 (lift coefficient):

The speed, pressure, drag and lift contour coefficients were analyzed. As can be seen in Figures 5 and 6, speed in red color area exceeded the inlet and according to bernolli, equation pressure must be decreased. This is obviously clear in pressure contour. This existing pressure difference in up and down pressure contour of the airfoil was the lift force parameter.

b) For angle of attack of α=6°, C_d=1.546*1000(drag coefficient) and C_l= 1.314*1000 (lift coefficient):

As can be seen in Figures 7 and 8, the pressure variation on the airfoil is more than the last condition which caused an increase in pressure difference and the lift coefficient rise. In pressure contour, it is observed that a high pressure mass was created in front of the airfoil that caused an increase in drag coefficient. The lift to drag coefficient proportion was approximately 0.85 which was an appropriate number.

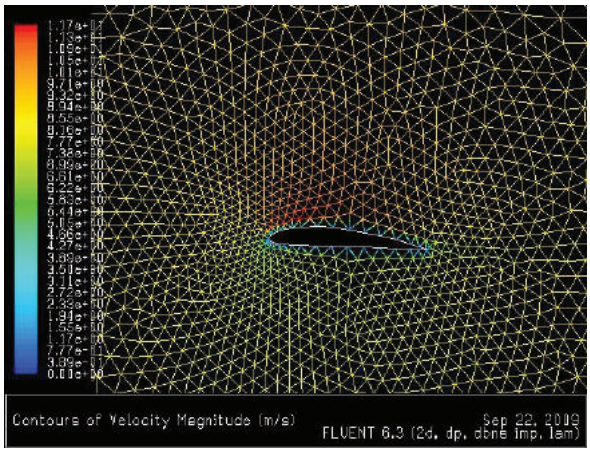

Figure 5: Speed contour in laminar flow (angle of attack of 4°)

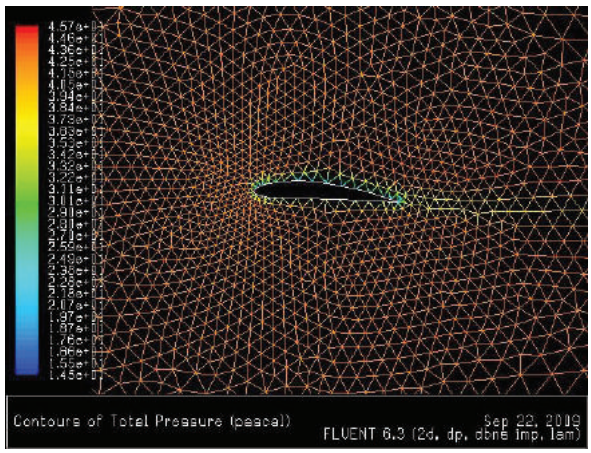

Figure 6: Pressure contour in laminar flow (angle of attack of 4°)

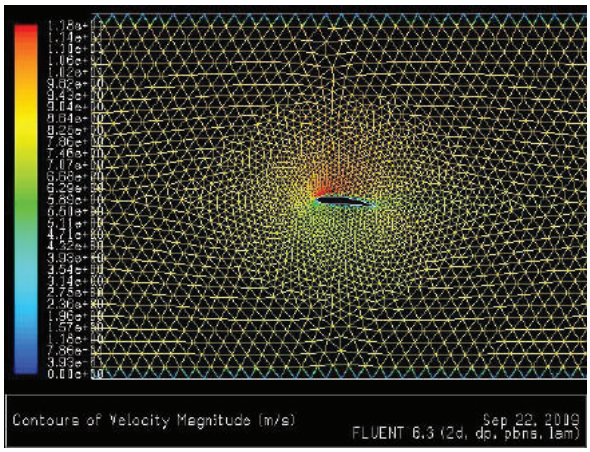

Figure 7: Speed contour in laminar flow (angle of attack of 6°)

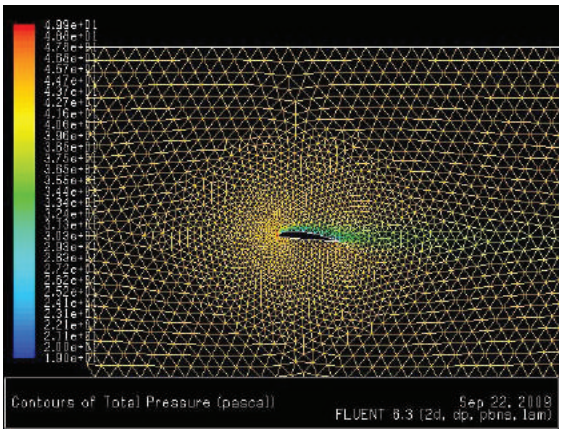

Figure 8: Pressure contour in laminar flow (angle of attack of 6°)

c) For the angle of attack of α=8°, C_d=1.836*1000(drag coefficient) and C_l= 1.314*1000 (lift coefficient):

In achieved contour from the angle of attack of 8°, the speed rose and the pressure reduction was clear but the pressure variations around the airfoil was much more evident than the former condition. The non-slip principle was also true in all of the conditions of these contours. The speed and pressure contour in laminar flow under the angle of attack of 8° can be observed in Figures 9 and 10. Besides, the lift coefficient proportion to drag coefficient was approximately 0.72 which was an acceptable number.

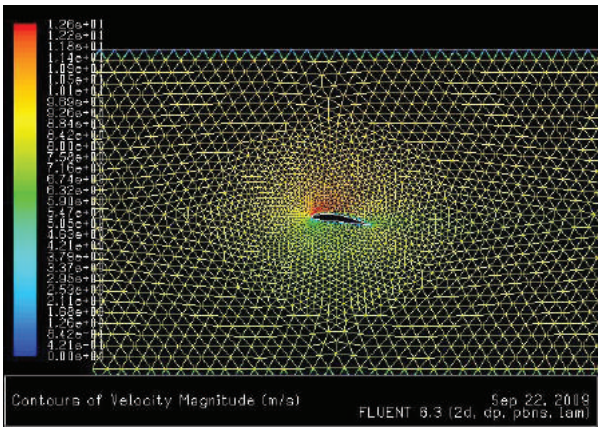

Figure 9: Speed contour in laminar flow (angle of attack of 8°)

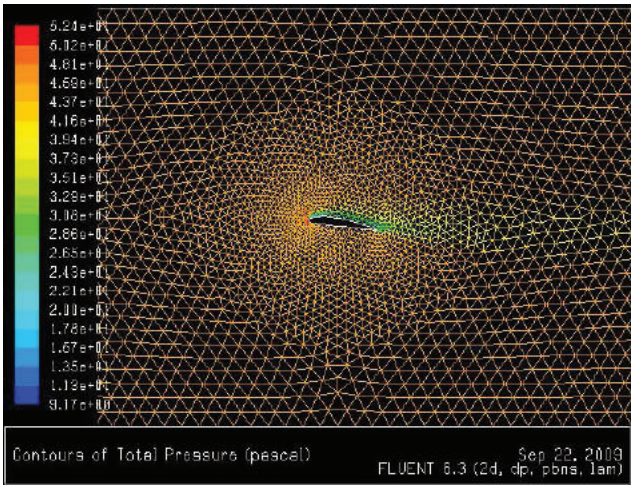

Figure 10: Pressure contour in laminar flow (angle of attack of 8°)

2. For turbulent flow condition: where the air speed was considered as 22.2 m/s and the water speed as 15m/s. Besides, this simulation was also conducted for three types of airfoils angle of attack 4°, 6° and 8° (lower part and in contact with flying boat).

a) For the angle of attack of α=4°, the achieved coefficients were as C_d=8.786*1000 (drag coefficient) and C_l=8.786*1000 (lift coefficient).

An increase in speed in turbulent condition was more than laminar condition and the pressure variations around the airfoil were increased. The lift and drag coefficients became more than six times due to these much variations. Figures 11 and 12 show the speed and pressure contours of the airfoil with the angle of attack of 4° for turbulent flow.

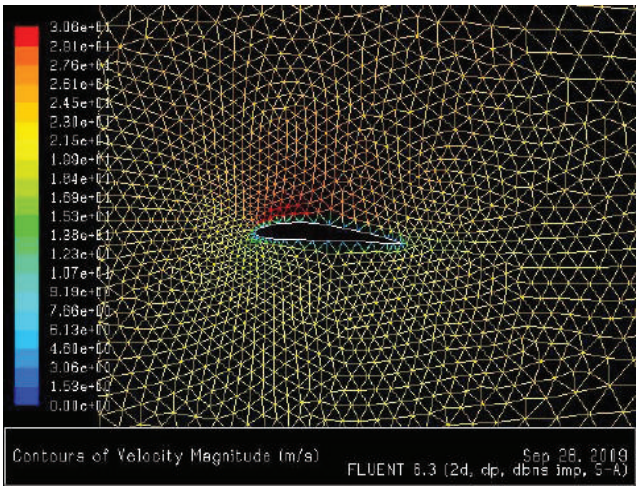

Figure 11: Speed contour in turbulent flow (angle of attack of 4°)

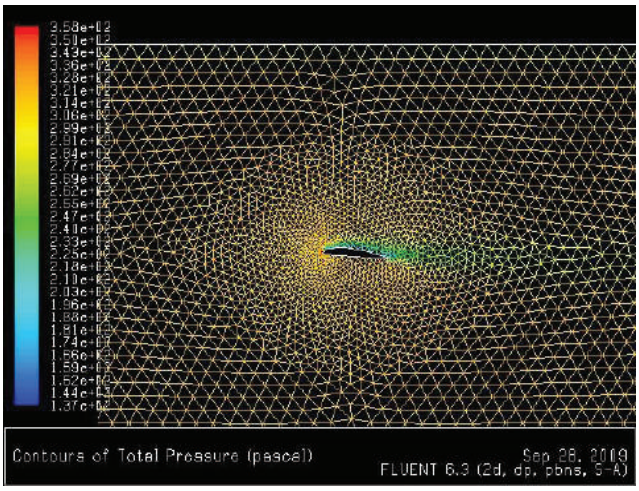

Figure 12: Pressure contour in turbulent flow (angle of attack of 4°)

b) For the angle of attack of α=6°, C_d=1.088*1000(drag coefficient) and C_l= 1.088*1000 (lift coefficient):

In Figures 13 and 14, the pressure around the airfoil had much more variations than the laminar condition and these condition variations result from turbulent terms due to high movement speed and their noises.

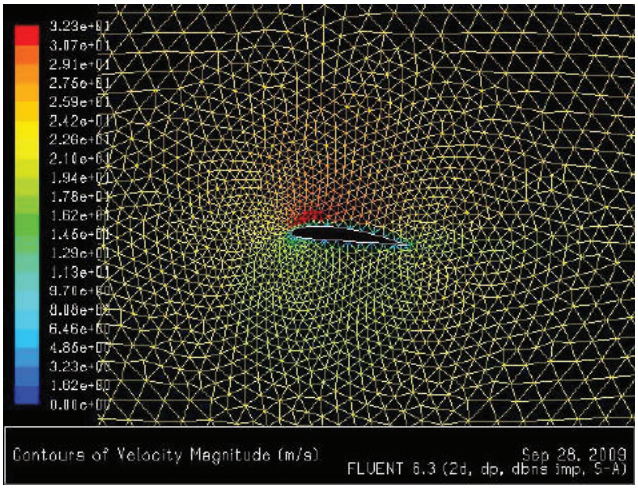

Figure 13: Speed contour in turbulent flow (angle of attack of 6°)

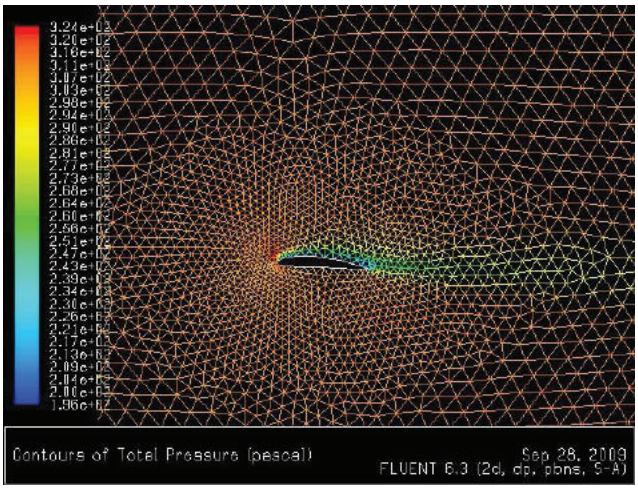

Figure 14: Pressure contour in turbulent flow (angle of attack of 6°)

c) For the angle of attack of α=8°, C_d=1.224*1000(drag coefficient) and C_l= 1.224*1000 (lift coefficient):

The interesting and important point in turbulent flow was that the lift and drag coefficients became the same and our intended cross section was the determiner of the lift and drag forces as shown in Figures 15 and 16.

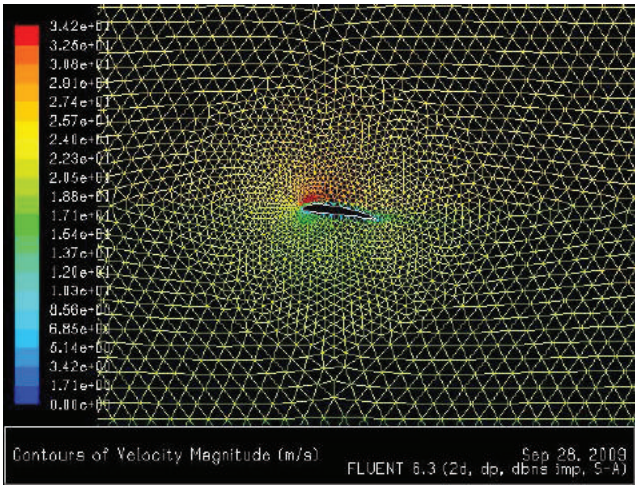

Figure 15: Speed contour in turbulent flow (angle of attack of 8°)

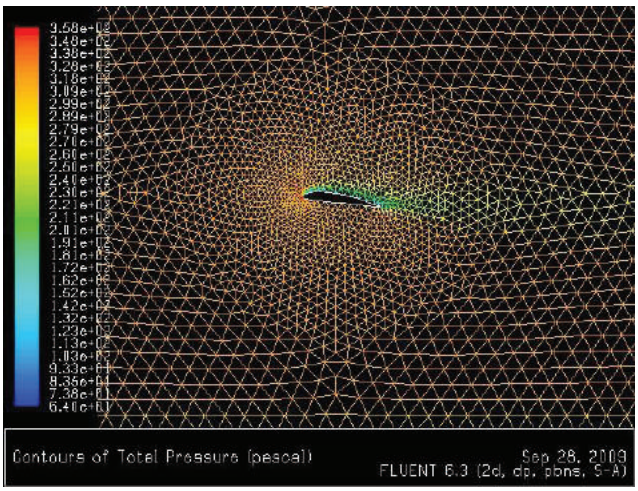

Figure 16: Pressure contour in turbulent flow (angle of attack of 8°)

3.1 The analysis of the amphibious vessel airfoil from the front view (with T=3 estuary water) under the turbulent flow

For the present investigation the air speed was 8.34 m/s and the sea water speed was considered 5m/s. For a part of vessel which is exposed to air, the drag coefficient was calculated as C_d=3.114*1000 Figure 17 shows the airfoil estuary water from the lateral view. The results indicated that in turbulent condition as can be seen from the pressure contour, the blue part which had a pressure of under 1 atm became less and tended towards under the aircraft tail. Therefore,

speed increase range in turbulent condition was more than laminar flow condition. Figures 17 and 18 show the pressure and speed contours under turbulent flow for the airfoil cross section in front view.

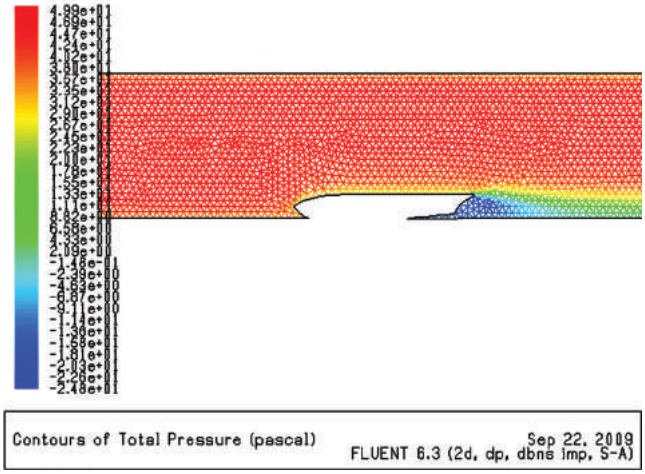

Figure 17: Pressure contour in turbulent flow (airfoil from lateral view)

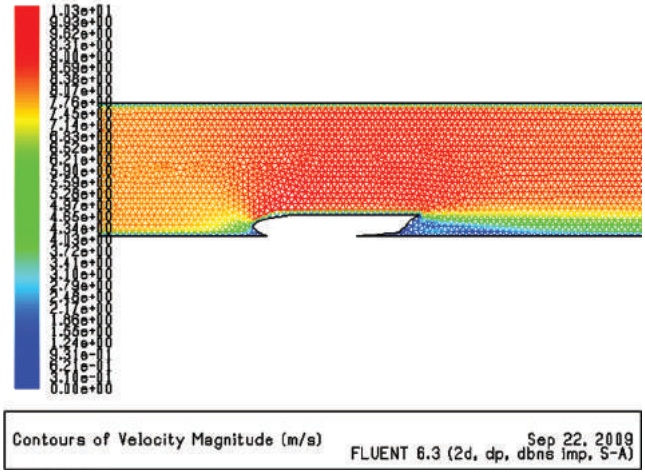

Figure 18: Speed contour in turbulent flow (airfoil from lateral view)

4.0 CONCLUSION

In this paper, based on engineering relations of the marine vessels and hydrodynamic stability of floating objects, first by considering the lower area geometry of an amphibious aircraft (flying boat) prevailing mathematical relations are addressed. Then, regarding to the simulation of the airfoil cross sections and contact surface with water in Fluent, the results are investigated and analyzed. Graphs in two laminar and turbulent (jumpy) flow stages are analyzed. As the angle of attack of airfoil has a tremendous effect on the achieved lift and drag coefficients, the angles of attack of 4°, 6° and 8° are considered for the simulation. The results show that the extracted speed and pressure contours by the Fluent are symmetrical which gave a positive point in designing this type of flying boat. In turbulent flow in which the angles of attacks of 6° and 8° are chosen, lift and drag coefficients show the same values. Therefore, the lift to drag coefficients proportion will be 1 which proves the sustainability of this aircraft type at high Reynolds numbers. Besides, in laminar flow for angles of attacks of 6° and 8°, the lift and drag coefficients have been achieved which indicate that dynamic stability of the vessel in both angles of attack types and the results show the same dynamic balance of the analysis with experimental results.

REFERENCES

[1] A. Stephan, F. Holzäpfel, T. Misaka, R. Geisler and R. Konrath, "Enhancement of Aircraft Wake Vortex Decay in Ground Proximity", CEAS Aero. J., Vol. 5, pp. 109-125, Jun. 2014.

[2] T. Y. Hubel, N. I. Hristov, Sh. M. Swartz and K. S. Breuer, "Time-Resolved Wake Structure and Kinematics of Bat Flight", Exp. Fluid., Vol. 46, pp. 933-943, Feb. 2009.

[3] M. Negahdari, Sh. Janbaz, A. Gharechahi and E. Shafiezadeh, "Hydrodynamic Analysis of The Vessel Movements By Using The Investigation Of Added Mass Effect In Fast Vessels", The first National Conference of Mokran Coasts and the Marine Authority of The Islamic Republic of Iran, 2012.

[4] M. S. Seif, M. Reishahri, M. Rahimian and J. R. Shahraki, "Suggested Proposal to Conduct Vessels Maneuver Tests", 9th Conference of Marine Industries, 2007.

[5] CH. Badoe, A. Phillips and R. Stephen, "Influence of Drift Angle on The Computation of Hull–Propeller–Rudder Interaction", Turnock Fluid Structure Interactions Research Group, Faculty of Engineering and the Environment, University of Southampton, 2015.

[6] M. Felli, S. Grizzi and M. Falchi, "Hydrodynamic and Hydroacoustic Phenomena in the Propeller Wake-Rudder Interaction", 33rd International Conference on Ocean, Offshore and Arctic Engineering, pp. 760–788, 2014.

[7] M. Safari,"Experimental And Numerical Investigation of Laser Forming of a Doubly Curved Saddle Shape With Spiral Irradiating Scheme", *J. Adv. Manuf. Tech.* Vol. 9, pp. 51-60, 2015.

[8] SH. Dehghan, M. Loh-Mousavi, M. Farzin and M. Safari, "Laser Forming of Metallic Dome-Shaped Parts Using Spiral And Radial- Circular Scan Paths", *J. Adv. Manuf. Tech.*, Vol. 10, pp. 29-44, 2016.